ACS APPLIED MATERIALS & INTERFACES

Research Article

www.acsami.org

Modification of Silver/Single-Wall Carbon Nanotube Electrical Contact Interfaces via Ion Irradiation

Nathanael D. Cox,[†,‡] Cory D. Cress,[§] Jamie E. Rossi,[‡,∥] Ivan Puchades,[‡,∥] Andrew Merrill,[‡,∥] Aaron D. Franklin,[⊥] and Brian J. Landi*[,‡,∥]

[†]Department of Microsystems Engineering, Rochester Institute of Technology, Rochester, New York 14623, United States
[‡]NanoPower Research Laboratories, Rochester Institute of Technology, Rochester, New York 14623, United States
[§]Electronics Science and Technology Division, United States Naval Research Laboratory, Washington, D.C. 20375, United States
[∥]Department of Chemical Engineering, Rochester Institute of Technology, Rochester, New York 14623, United States
[⊥]Departments of Electrical & Computer Engineering and Chemistry, Duke University, Durham, North Carolina 27708, United States

ABSTRACT: Introduction of defects via ion irradiation ex situ to modify silver/single-wall carbon nanotube (Ag-SWCNT) electrical contacts and the resulting changes in the electrical properties were studied. Two test samples were fabricated by depositing 0.1 μm Ag onto SWCNT thin films with average thicknesses of 10 and 60 nm, followed by ion irradiation (150 keV $^{11}B^+$ at 5×10^{14} ions/cm^2). The contact resistance (R_c) between the Ag and SWCNT thin films was determined using transfer length method (TLM) measurements before and after ion irradiation. R_c increases for both test samples after irradiation, while there is no change in R_c for control structures with thick Ag contacts (1.5 μm), indicating that changes in R_c originate from changes in the SWCNT films and at the Ag-SWCNT interface caused by ion penetration through the Ag contact electrodes. R_c increases by ~4× for the 60 nm SWCNT structure and increases by ~2.4× for the 10 nm SWCNT structure. Raman spectroscopy measurements of the SWCNTs under the contacts compared to the starting SWCNT film show that the degradation of the 10 nm SWCNT structure was less significant than that of the 60 nm SWCNT structure, suggesting that the smaller change in R_c for the 10 nm SWCNT structure is a result of the thickness-dependent damage profile in the SWCNTs. Despite the increase in overall contact resistance, further TLM analysis reveals that the specific contact resistance actually decreases by ~3.5−4× for both test samples, suggesting an enhancement of the electrical properties at the Ag-SWCNT interface. Irradiation simulations provide a physical description of the underlying mechanism, revealing that Ag atoms are forward-scattered into the SWCNTs, creating an Ag/C interfacial layer several nanometers in depth. The collective results indicate competing effects of improvement of the Ag-SWCNT interface versus degradation of the bulk SWCNT films, which has implications for scaled high-performance devices employing thinner SWCNT films.

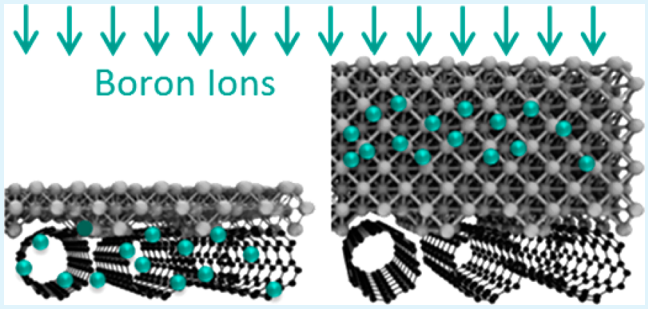

KEYWORDS: *single-wall carbon nanotubes, silver electrodes, contact resistance, defects, nanomaterials, transfer length method, Raman spectroscopy*

INTRODUCTION

Metal contacts to single-wall carbon nanotubes (SWCNTs) are essential in a majority of SWCNT-based electronic devices, including organic photovoltaics,[1,2] CNT-metal matrix composite electrodes for advanced solar cells,[3,4] thin-film transistors,[5] and scaled high performance field effect transistors.[6] As the SWCNT layers are dimensionally decreased in these advanced devices, the effects of the electrical contact between metals and CNTs become increasingly important. For instance, the contact resistance becomes dominant for scaled field effect transistors.[7,8] Many of these devices are intended for use in space and other harsh radiation environments, and it is thus critical to understand changes in the metal-CNT electrical interactions as a result of different types of radiation, including ion irradiation.

Many studies have investigated the effects of ion irradiation on a wide range of SWCNT materials, including SWCNT papers,[9,10] electronic-type separated[11] and diameter controlled[12] SWCNT thin films, and many other SWCNT types and form factors,[13−17] yet no studies have specifically investigated the role that SWCNT−metal contacts play in measured results. Specifically, the effects of ion irradiation on the contact resistance between metals and SWCNTs have not been documented, which is critical for harsh environment applications. In the work presented here, modification of the metal-SWCNT interface by exposure to ion irradiation was

Received: November 2, 2016
Accepted: February 3, 2017
Published: February 3, 2017

DOI: 10.1021/acsami.6b14041
ACS Appl. Mater. Interfaces 2017, 9, 7406−7411

investigated. A method was developed to determine whether ions impact the contact resistance and other electrical transport properties at the SWCNT−metal interface. Different Ag contact thicknesses were deposited on SWCNT films to provide a means to control the ion irradiation-induced damage at the SWCNT−metal contact using 150 keV $^{11}B^+$, either stopping them within the Ag contacts or allowing the ions to penetrate fully through to the underlying SWCNTs. For thinner Ag contacts where ion penetration is expected, two different SWCNT film thicknesses were utilized to explore the effect of SWCNT film thickness on the measured results. Transfer length method (TLM) measurements and analysis were used to quantify changes in contact resistance, transfer length, and specific contact resistance in response to ion irradiation. These observations along with computer simulations provide an understanding of how defect generation within the structures affects the properties of the Ag-SWCNT interface and additionally accounts for the role of metal thickness and SWCNT film thickness.

EXPERIMENTAL SECTION

Structures were fabricated for performing TLM measurements to extract the Ag-SWCNT contact resistance. In this study, high purity SWCNT materials were synthesized in-house by laser vaporization and purified using established techniques.[18] The diameter range of SWCNTs was 1.0−1.4 nm based on Raman spectroscopy analysis.[12] Thin films of the high purity SWCNTs were transferred onto Si/SiO_2 substrates using a standard mixed cellulose ester film transfer method.[19,20] Ag contacts for TLM measurements were deposited onto the SWCNT films via thermal evaporation (Kurt Lesker PVD 75C) through a shadow mask. Figure 1a shows a schematic detailing a top-down view of the surface of the TLM structure with Ag contact dimensions of 2 × 8 mm ($L \times W$) and SWCNT channel lengths (d_1−d_4) of 1, 2, 3, and 4 mm. Three TLM structures were produced in total: (1) a control sample with 1.5 μm Ag contacts on a 60 nm SWCNT film (Figure 1b), (2) a test sample with 0.1 μm Ag contacts deposited onto a 60 nm SWCNT film (Figure 1c), and (3) a test sample with 0.1 μm Ag contacts deposited onto a 10 nm SWCNT film (Figure 1d). The average SWCNT thicknesses were determined by profilometry using a Tencor P2 Profilometer. TLM measurements were performed on the samples after metal contact deposition. The shadow mask was then carefully placed back onto the sample to shield the SWCNTs in the channel regions from subsequent ion irradiation. The realignment of the shadow mask was confirmed by optical microscopy. The samples were then irradiated with 150 keV $^{11}B^+$ (Varian 350D medium current ion implanter) at 5×10^{14} ions/cm^2, as illustrated in Figures 1b−d. The shadow mask was selected to be of sufficient thickness (0.5 mm) to mask the SWCNTs in the channel (between the Ag contacts) from the incident ions so that only the Ag contacts are irradiated. Following ion irradiation, TLM measurements were repeated to assess changes in the contact resistance in response to ion irradiation.

TLM measurements were performed by forcing current between each pair of electrodes and monitoring the voltage, and the resistance was calculated via Ohm's law. Raman spectroscopy of the SWCNTs was performed both in the channel (shielded from irradiation) and under the contacts using a LabRam spectrometer at 633 nm excitation (Jobin Yvon Horiba). Kapton tape was used to peel the Ag contacts off of the SWCNTs to enable Raman measurements of the SWCNTs under the contacts.

RESULTS

The Ag contact thicknesses were specifically chosen for two intended scenarios: (1) the ions come to rest within the thick contacts, and (2) the ions are transmitted through the thin contacts into the SWCNT film and SiO_2. The range of ions in

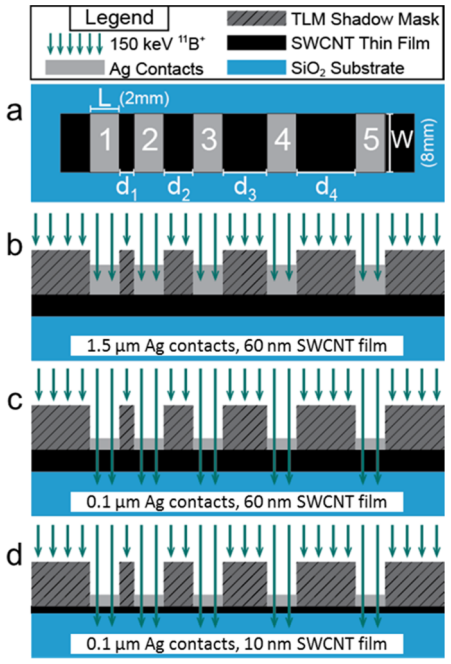

Figure 1. (a) Schematic showing a top-down view of structures fabricated for TLM measurements of contact resistance between Ag contacts (labeled 1−5) and SWCNT thin films with contact lengths L and widths W of 2 and 8 mm, respectively, and electrodes spaced a distance d apart. (b−d) Cross-sectional views showing TLM structures with Ag contacts during ion irradiation with the TLM shadow mask in place so that the channel region is shielded and the 150 keV $^{11}B^+$ are only incident on the Ag contacts. The samples consist of (b) 1.5 μm Ag contacts on a 60 nm SWCNT film, (c) 0.1 μm Ag contacts on a 60 nm SWCNT film, and (d) 0.1 μm Ag contacts on a 10 nm SWCNT film.

metals will vary depending on factors such as the ion species, energy, and metal type. $^{11}B^+$ was selected for the present experiments to enable comparisons to previous work that examined changes in the structural and electronic degradation of electronic-type separated[11] and diameter enriched[12] SWCNTs under 150 keV $^{11}B^+$ irradiation. SRIM software[21] was used to calculate the range of 150 keV $^{11}B^+$ in Ag (conditions for the present experiments) to ensure that the proper Ag contact thicknesses were selected. The projected range of $^{11}B^+$ in Ag is approximately 0.18 ± 0.09 μm. Thus, thin Ag contacts of 0.1 μm (test samples) and thick Ag contacts of 1.5 μm (control samples) were deposited to meet the given criteria of contacts either below or well above the projected $^{11}B^+$ range, respectively. Such an experimental setup ensures that changes in contact resistance after irradiation can be distinguished as resulting from either ion-induced damage in the Ag or ion-induced damage in the SWCNT film.

TLM measurements of the structures described in Figure 1 were performed before and after ion irradiation to discern whether the ions have any impact on R_c. The results of the TLM measurements are shown in Figure 2, where the measured electrical resistance is plotted versus contact spacing for the control sample, the 60 nm SWCNT structure, and the 10 nm SWCNT structure (Figures 2a−c, respectively). The closed black squares are the measured resistance before ion-irradiation, and the open red squares are the measured resistance after ion-irradiation, with dotted lines corresponding to linear least-squares fits to each data set (all linear fits exhibit

DOI: 10.1021/acsami.6b14041
ACS Appl. Mater. Interfaces 2017, 9, 7406−7411

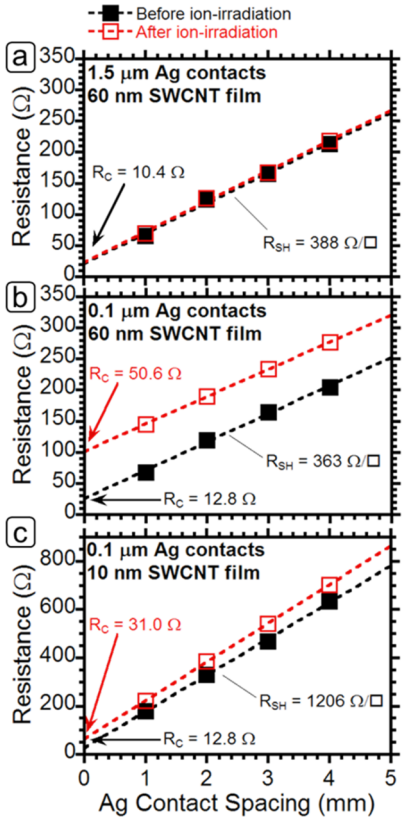

Figure 2. Plots of the measured 4-point resistance versus Ag electrode spacing for TLM structures with (a) 1.5 μm Ag contacts on a 60 nm SWCNT film, (b) 0.1 μm Ag contacts on a 60 nm SWCNT film, and (c) 0.1 μm Ag contacts on a 10 nm SWCNT film. Resistance values for the structures are shown before (black square) and after (red squares) irradiation with 150 keV $^{11}B^+$ to a fluence of 5×10^{14} ions/cm^2. The linear fits of the data are indicated by dashed lines.

$R^2 > 0.996$). The linear fit to TLM measurements is used to determine the unknown variables by eq 1:[22]

$$R_{total} = \frac{R_{sh}}{W} d + 2R_c \quad (1)$$

where R_{total} is the total measured resistance, R_{sh} is the sheet resistance between the contacts, W the width of the contacts, and d the distance between consecutive contacts, as defined in Figure 1. The slope of the line is directly proportional to the sheet resistance, and the vertical intercept (R at $d = 0$) is $2R_c$. Previous work has shown that SWCNTs irradiated under the present 150 keV $^{11}B^+$ conditions should exhibit a fluence-dependent increase in R_{sh}.[11] No appreciable changes were observed in the slope of the linear fits to the data (and hence, R_{sh}) after ion irradiation, indicating that the shadow mask was properly realigned after the initial TLM measurements and serves as an effective radiation shield. As shown in Figure 2, the contact resistance before irradiation is identical for the 10 and 60 nm SWCNT structures (12.8 Ω) and similar to the control sample (10.4 Ω). After ion irradiation, R_c remains relatively unchanged for the control sample (1.5 μm contacts, Figure 2a) and increases for both test samples (0.1 μm contacts, Figures 2b and c). As noted previously, SRIM calculations show that the $^{11}B^+$ should stop well within the thick Ag contacts and should be transmitted through the thin contacts and the underlying SWCNT film. Thus, the increase in R_c after irradiation for the thin-contact structures suggests that the origin of the change is related to modifications of the SWCNTs and/or the Ag-SWCNT interface and eliminates the prospect of contributions from damaged Ag contacts. R_c increases by ~4× for the 60 nm SWCNT structure (Figure 2b) and ~2.4× for the 10 nm SWCNT structure (Figure 2c), indicating that changes in the measured contact resistance resulting from ion penetration through the contacts are dependent on the SWCNT film thickness.

Characterization of the SWCNT material properties can facilitate understanding of the observed changes in contact resistance of the Ag-SWCNT interface induced by ion irradiation. Raman spectroscopy was employed to evaluate structural damage in the SWCNTs under the contacts as well as in the channel region, which was shielded from the ion irradiation by the TLM shadow mask. Raman measurements underneath the contacts were facilitated by adhering Kapton tape to the Ag surface and peeling it back to reveal the bottom of the metal contact and top of the SWCNT film, as illustrated in Figure 3a. The regions between the contacts, which were shielded by the shadow mask, are labeled "shielded region", and the regions where the Ag contacts were exposed to radiation are labeled "under contacts". In some cases, portions of the SWCNT films adhered to the Ag upon contact removal; however, the Raman spectra of these SWCNTs were identical to those of the SWCNTs remaining on the substrate.

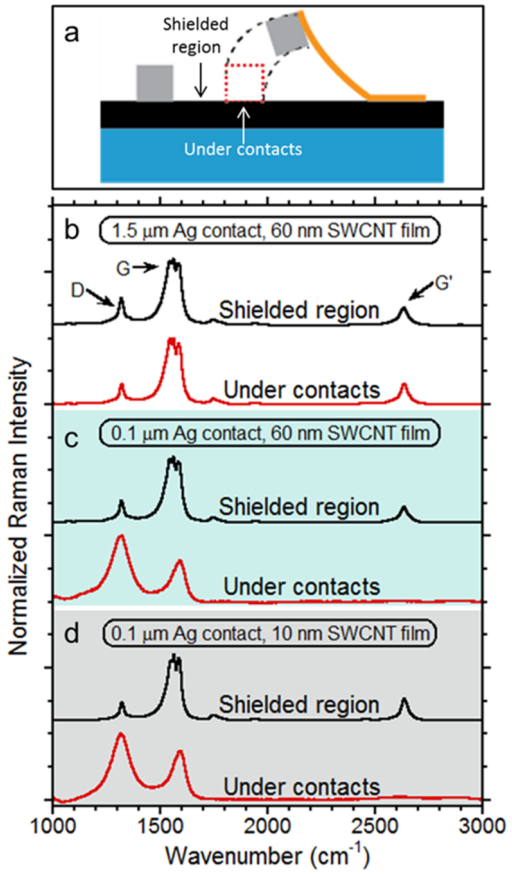

Figure 3. (a) Schematic illustration showing the removal of the contacts by Kapton tape to enable Raman measurements under the contacts. The channel region, which was shielded from ion irradiation, is labeled "shielded region". (b–d) Raman spectra for the shielded region and under the contacts are shown for each sample with the D-, G-, and G′-peaks labeled.

DOI: 10.1021/acsami.6b14041
ACS Appl. Mater. Interfaces 2017, 9, 7406–7411

The characteristic Raman peaks of interest for SWCNTs are the D-peak (~1300 cm^{-1}), which is related to defects, the G-peak (~1590 cm^{-1}), indicating sp^2 graphitization, and the G′-peak (~2690 cm^{-1}), corresponding to two-phonon scattering processes around the *K*-point.[23] Figure 3b shows the Raman spectra for the control sample (thick contacts) after irradiation. The Raman spectra both in the shielded region and under the contacts are nearly identical, indicating no significant changes in the SWCNT structural properties as a result of ion irradiation, which is expected from the SRIM calculations of projected range and the lack of changes in R_c. Figures 3c and d show the Raman spectra for the 60 and 10 nm SWCNT structures, respectively, after irradiation. The Raman spectra for the SWCNTs in the shielded regions are also nearly identical to the control sample spectra (Figure 3b); however, the Raman spectra under the contacts show significant changes in the prominent SWCNT peaks. The extent of structural damage (i.e., defect density) within the SWCNTs can be evaluated by examining relative changes in the Raman peak ratios after ion irradiation, e.g., $[D/G(\Phi)]/[D/G(0)]$, where $D/G(\Phi)$ is the D/G-peak ratio under the contacts, and $D/G(0)$ is the D/G-peak ratio in the shielded region. $[D/G(\Phi)]/[D/G(0)]$ is 4.8 for the 60 nm SWCNT structure and 4.1 for the 10 nm SWCNT structure. In comparison, nearly complete suppression of the G′-peak in the SWCNTs under the contacts is observed, resulting in $[D/G'(\Phi)]/[D/G'(0)]$ values of 54 for the 60 nm SWCNT structure and 24 for the 10 nm SWCNT structure. The collective Raman results indicate structural damage of the SWCNTs under the contacts for both test samples but less significant degradation of the 10 nm SWCNT structure.

DISCUSSION

There is a clear correlation of structural damage in the SWCNT films to the increase in R_c for both test samples, but analysis of the transfer length (L_t) and the specific contact resistance (ρ_c) is needed to assess these effects as they relate to the Ag-SWCNT interface. L_t is the length in the direction of current over which $1/e$ of the current has been extracted from the contacts, and ρ_c is the area-normalized resistivity of the interface.[24] As defined by the transmission line model, L_t and ρ_c are independent of the contact area and are a property of the metal-SWCNT interface. If the contact length is >1.5 L_t and the sheet resistance under the contacts is identical to the sheet resistance in the channel (an assumption that cannot be verified), then eq 1 can be approximated as[22]

$$R_{total} = \frac{R_{sh}}{W}d + 2R_c \approx \frac{R_{sh}}{W}(d + 2L_t) \quad (2)$$

The contacts used in the present study have a length of 2 mm, ensuring the validity of eq 2, because L_t is typically on the order of micrometers for contacts to SWCNT films. Solving eq 2 for L_t leads to

$$L_t = \frac{WR_c}{R_{sh}} \quad (3)$$

By the definition of the transfer length, the specific contact resistance can be expressed as[24]

$$\rho_c = R_{sh}(L_t)^2 \quad (4)$$

Thus, from the TLM data, the value of L_t can be determined using eq 3, and ρ_c can be determined using eq 4. However, for cases in which the sheet resistance under the contacts is modified, eq 2 is no longer valid because of the addition of an extra series resistance for current in the SWCNT film under the contact traveling toward the channel, leading to an alternative expression of eq 2 as[24]

$$R_{total} = \frac{R_{sh}}{W}d + 2R_c \approx \frac{R_{sh}}{W}d + \frac{2R_{sk}L_t}{W} \quad (5)$$

where R_{sk} represents the sheet resistance under the contacts. For this scenario, L_t is now determined by a modified expression of eq 3 as

$$L_t = \frac{WR_c}{R_{sk}} \quad (6)$$

and ρ_c is determined by a modified expression of eq 4 as

$$\rho_c = R_{sk}(L_t)^2 \quad (7)$$

In most cases, it is not possible to know the sheet resistance under the contacts, and thus additional measurements are needed to determine L_t and ρ_c. This scenario is commonly seen where modifications have been made to achieve Ohmic metal–semiconductor contacts such as silicide contacts.[24,25] Typically, in these cases, R_c, L_t, and ρ_c decrease as a result of improving the contact interface. However, removal of the contacts in the present study permits calculation of R_{sk} from the changes in the Raman D/G′-peak ratios. Previous work[11,12] has shown that the relative increase in sheet resistance at a given fluence correlates linearly with the relative increase in D/G′-peak ratios (i.e., $[D/G'(\Phi)]/[D/G'(0)] \cong [R_{sh}(\Phi)]/[R_{sh}(0)]$). Thus, based on the measured $[D/G'(\Phi)]/[D/G'(0)]$ values for each test sample, the sheet resistance under the contacts increases (relative to the sheet resistance in the channel) by ~54× for the 60 nm SWCNT structure and ~24× for the 10 nm SWCNT structure. Table 1 provides a summary of the calculated TLM values for the test samples both before and after irradiation and provides details on how those values are determined. The measured values for the 10 nm SWCNT structure are fairly consistent with other work for SWCNTs synthesized via arc discharge with film thicknesses of 20–30 nm, which reported 80 μm and 0.02 Ω cm^2 for L_t and ρ_c, respectively.[1] The transfer length and specific contact resistance decrease similarly for both samples after irradiation. For example, ρ_c decreases by 3.5× for the 60 nm SWCNT structure and by 4.1× for the 10 nm SWCNT structure. Overall, the decreases in L_t and ρ_c suggest that the irradiation-induced damage improves the electrical properties of the Ag-SWCNT interface despite the increase in contact

Table 1. Electrical Values for 0.1 μm Ag Contacts on 60 nm and 10 SWCNT Films Both As-Deposited and after Ion Irradiation with 150 keV $^{11}B^+$ to a Fluence of 5 × 10^{14} ions/cm^2

		R_{sh} or R_{sk} (Ω/□)	R_C (Ω)	L_T (μm)	ρ_c (Ωcm^2)
60 nm-thick SWCNT film	as-deposited	363[a]	12.8	281.7[b]	0.29[c]
	irradiated	19 500[d]	50.6	20.6[e]	0.08[f]
10 nm-thick SWCNT film	as-deposited	1206[a]	12.8	84.7[b]	0.09[c]
	irradiated	29 320[d]	31.0	8.5[e]	0.02[f]

[a]Determined from eq 1. [b]Determined from eq 3. [c]Determined from eq 4. [d]Calculated from relative changes in D/G′-ratios after irradiation. [e]Determined from eq 6. [f]Determined from eq 7.

DOI: 10.1021/acsami.6b14041
ACS Appl. Mater. Interfaces 2017, 9, 7406–7411

resistance. Thus, the overall measured increase in R_c for both test samples is a result of adding a series resistance between the Ag-SWCNT interface and the SWCNTs in the channel region, and this increase in resistance dominates over any potential benefits gained by electrical enhancement of the Ag-SWCNT interface. However, the less significant increase in R_c for the 10 nm SWCNT structure results from a less significant increase in sheet resistance (24×) under the contacts compared to the increase in sheet resistance (54×) for the thicker 60 nm SWCNT film. Clearly, the effects of ion irradiation on the Ag-SWCNT electrical properties are dependent on the SWCNT film thickness.

SRIM simulations were employed to gain additional insight into the physical mechanism for the enhancement of L_t and ρ_c at the Ag-SWCNT interface. The transport of ion in matter (TRIM) program within SRIM was used to simulate 150 keV $^{11}B^+$ collisions into a Ag/C/SiO_2 (100/70/250 nm) target using detailed collisions with full damage cascades, 40 000 particle histories, and assuming a C density of 0.5 g/cm^3 and displacement energy of 20 eV.[12] Analysis of the incident $^{11}B^+$ and recoil distributions in the SWCNT layer was performed with data from the Range output files. Figure 4a shows the

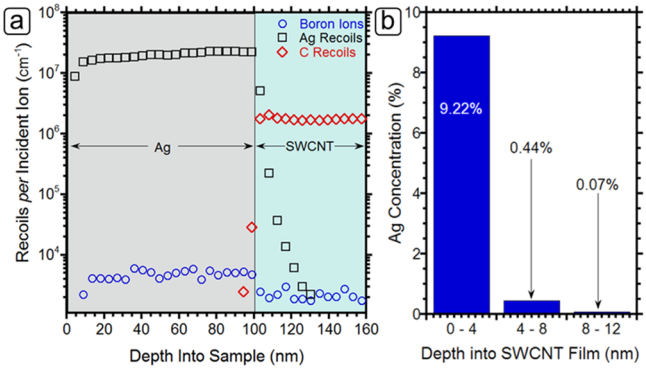

Figure 4. Results of TRIM simulations for 150 keV $^{11}B^+$ into a Ag/C/SiO_2 (100/100/250 nm) target showing (a) $^{11}B^+$, Ag recoil, and C recoil distributions plotted versus depth into the Ag and SWCNT layers and (b) concentration of Ag atoms in the SWCNT film.

distributions of B ions and final location of Ag and C recoils vs depth into the sample, which are defined as the number of recoils per incident B ion per cm. The data reveal a high distribution of forward-scattered Ag (relative to C and $^{11}B^+$) in the top ~4 nm (sample depth of 104 nm) of the SWCNT film. Multiplying any ion/recoil distribution by the dose (5×10^{14} ions/cm^2) gives an atomic density distribution (i.e., atoms/cm^3) which can be converted into an atomic ratio by dividing by the total atomic density of the layer. The calculated results are plotted as Ag concentration vs depth into the SWCNT film in Figure 4b. Interestingly, from 100 to 104 nm (4 nm into the C layer), the average Ag concentration was 9.2% (or 9.2×10^4 ppm), decreasing dramatically to 0.44% from 4–8 nm and 0.07% form 8–12 nm into the SWCNT film. In contrast, the $^{11}B^+$ concentration is <50 ppm throughout the Ag and SWCNT layers because most of the boron ions are transmitted through the SWCNT film and into the SiO_2. Thus, any doping effects from the $^{11}B^+$ will be negligible, especially given that substitutional doping of CNTs is very difficult to achieve and requires ion energies on the order of 70–500 eV,[15] much lower than the current experimental conditions. The C concentration in the Ag layer is also <50 ppm except at a sample depth of 96–100 nm (directly before the Ag-SWCNT interface) where the concentration is ~245 ppm due to backscattered C. Analysis of the ion and recoil distributions reveals forward scattered Ag atoms at the Ag-SWCNT interface, suggesting the existence of an Ag/C (~9/91%) interfacial layer with improved electrical interactions with the Ag contacts. The existence of such an interfacial layer also provides insight into the overall observations regarding SWCNT film thickness: the relative contribution of the interface behavior on the measured contact properties should increase with decreasing SWCNT film thickness. For example, this electrically enhanced Ag/C layer comprises an order of magnitude higher portion of the 10 nm SWCNT film compared to the 60 nm SWCNT film. Thus, it is likely that use of SWCNT active layers approaching monolayer thickness would further modify the R_c values as a result of the relative contribution of the enhancement of L_t and ρ_c and the observed trend of smaller damage profiles for thinner SWCNT films.

CONCLUSIONS

The effects of ion irradiation on the Ag-SWCNT interface were studied, and results show that exposure to extreme ion irradiation can significantly impact the electrical properties of SWCNT–metal contacts. For structures with 0.1 μm Ag contacts deposited on 60 and 10 nm SWCNT film thicknesses, irradiation with 5×10^{14} $^{11}B^+$/cm^2 causes the contact resistance to increase by 4× and 2.4×, respectively. The contact resistance did not change for control structures with thick Ag contacts (1.5 μm) where the $^{11}B^+$ ions are expected to stop within the metal contact and not affect the Ag-SWCNT interface. Thus, the changes in R_c are directly correlated to structural damage in the SWCNTs, as confirmed by Raman spectroscopy measurements. Further analysis shows decreases of ~10–13× in transfer length and ~3.5–4× in specific contact resistance. This infers that transport at the Ag-SWCNT interface was actually improved by the ion irradiation, while transport through the SWCNTs was degraded. Analysis of the ion and recoil distributions from SRIM suggests that Ag atoms are forward-scattered into the Ag-SWCNT interface, creating an Ag/C (9/91%) interfacial layer ~4 nm in thickness, which may explain the improvement in the electrical properties of the Ag-SWCNT interface despite significant structural damage. The competing effects of interface enhancement and bulk SWCNT degradation show a dependence on SWCNT layer thickness with the thinner SWCNT film experiencing less structural damage and a smaller increase in R_c. Overall, this study provides a framework to investigate the effects of various ion species, energies, metal compositions, and SWCNT layer thicknesses on the electrical interactions between metals and SWCNTs, all of which are important considerations for devices exposed to extreme ion irradiation conditions.

AUTHOR INFORMATION

Corresponding Author

*E-mail: brian.landi@rit.edu.

ORCID

Nathanael D. Cox: 0000-0003-0843-9141

Notes

The authors declare no competing financial interest.

DOI: 10.1021/acsami.6b14041
ACS Appl. Mater. Interfaces 2017, 9, 7406–7411

■ ACKNOWLEDGMENTS

The authors gratefully acknowledge funding from the U.S. government and through the Defense Threat Reduction Agency (DTRA) under Grant HDTRA-1-10-1-0122, the Office of Naval Research under Grant N00014-15-1-2720, and the Air Force Research Laboratory under Agreement FA9453-14-1-0232. This project was also partially supported by a grant from the Intelligence Community Postdoctoral Research Fellowship Program through funding from the Office of the Director of National Intelligence. All statements of fact, opinion, or analysis expressed are those of the authors and do not reflect the official positions or views of the Intelligence Community or any other U.S. government agency. Nothing in the contents should be construed as asserting or implying U.S. government authentication of information or Intelligence Community endorsement of the authors' views.

■ REFERENCES

(1) Jackson, R.; Graham, S. Specific Contact Resistance at Metal/Carbon Nanotube Interfaces. *Appl. Phys. Lett.* **2009**, *94*, 1−3.
(2) Jackson, R. K.; Munro, A.; Nebesny, K.; Armstrong, N.; Graham, S. Evaluation of Transparent Carbon Nanotube Networks of Homogeneous Electronic Type. *ACS Nano* **2010**, *4*, 1377−1384.
(3) Cox, N. D.; Rape, A.; Pham, M.; Rossi, J. E.; Bucossi, A. R.; Landi, B. J. Free-Standing Silver/Carbon Nanotube Metal Matrix Composite Thin Films. *J. Mater. Sci.* **2016**, *51*, 10935−10942.
(4) Phillips, A. B.; Tompkins, B. L.; Song, Z.; Khanal, R. R.; Liyanage, G. K.; Gapp, N. D.; Wilt, D. M.; Heben, M. J. Carbon Nanotube Reinforced Cu Metal Matrix Composites for Current Collection from Space Photovoltaics. *IEEE Photovoltaic Spec. Conf.* **2015**, 1−5.
(5) Wang, H. L.; Koleilat, G. I.; Liu, P.; Jimenez-Oses, G.; Lai, Y. C.; Vosgueritchian, M.; Fang, Y.; Park, S.; Houk, K. N.; Bao, Z. N. High-Yield Sorting of Small-Diameter Carbon Nanotubes for Solar Cells and Transistors. *ACS Nano* **2014**, *8*, 2609−2617.
(6) Franklin, A. D.; Chen, Z. Length Scaling of Carbon Nanotube Transistors. *Nat. Nanotechnol.* **2010**, *5*, 858−862.
(7) Franklin, A. D.; Farmer, D. B.; Haensch, W. Defining and Overcoming the Contact Resistance Challenge in Scaled Carbon Nanotube Transistors. *ACS Nano* **2014**, *8*, 7333−7339.
(8) Franklin, A. D. Nanomaterials in Transistors: From High-Performance to Thin-Film Applications. *Science* **2015**, *349*, 2750.
(9) Cress, C. D.; Schauerman, C. M.; Landi, B. J.; Messenger, S. R.; Raffaelle, R. P.; Walters, R. J. Radiation Effects in Single-Walled Carbon Nanotube Papers. *J. Appl. Phys.* **2010**, *107*, 014316.
(10) Skákalová, V.; Kaiser, A. B.; Dettlaff, U.; Arstila, K.; Krasheninnikov, A. V.; Keinonen, J.; Roth, S. Electrical Properties of C4+ Irradiated Single-Walled Carbon Nanotube Paper. *Phys. Status Solidi B* **2008**, *245*, 2280−2283.
(11) Rossi, J. E.; Cress, C. D.; Helenic, A. R.; Schauerman, C. M.; DiLeo, R. A.; Cox, N. D.; Messenger, S. R.; Weaver, B. D.; Hubbard, S. M.; Landi, B. J. Ion Irradiation of Electronic-Type-Separated Single Wall Carbon Nanotubes: A Model for Radiation Effects in Nanostructured Carbon (Vol 112, 034314, 2012). *J. Appl. Phys.* **2012**, *112*, 34134.
(12) Rossi, J. E.; Cress, C. D.; Merrill, A.; Soule, K. J.; Cox, N. D.; Landi, B. J. Intrinsic Diameter Dependent Degradation of Single-Wall Carbon Nanotubes from Ion Irradiation. *Carbon* **2015**, *81*, 488−496.
(13) Kaiser, A. B.; Skákalová, V.; Roth, S. Modelling Conduction in Carbon Nanotube Networks with Different Thickness, Chemical Treatment and Irradiation. *Phys. E (Amsterdam, Neth.)* **2008**, *40*, 2311−2318.
(14) Skákalová, V.; Kaiser, A. B.; Osváth, Z.; Vértesy, G.; Biró, L. P.; Roth, S. Ion Irradiation Effects on Conduction in Single-Wall Carbon Nanotube Networks. *Appl. Phys. A: Mater. Sci. Process.* **2008**, *90*, 597−602.
(15) Krasheninnikov, A. V.; Nordlund, K. Ion and Electron Irradiation-Induced Effects in Nanostructured Materials. *J. Appl. Phys.* **2010**, *107*, 071301.
(16) Liu, A. C. Y.; Arenal, R.; Montagnac, G. In Situ Transmission Electron Microscopy Observation of Kev-Ion Irradiation of Single-Walled Carbon and Boron Nitride Nanotubes. *Carbon* **2013**, *62*, 248−255.
(17) Osváth, Z.; Vértesy, G.; Tapasztó, L.; Wéber, F.; Horváth, Z.; Gyulai, J.; Biró, L. Atomically Resolved Stm Images of Carbon Nanotube Defects Produced by Ar+ Irradiation. *Phys. Rev. B: Condens. Matter Mater. Phys.* **2005**, *72*, 72.
(18) Landi, B. J.; Cress, C. D.; Evans, C. M.; Raffaelle, R. P. Thermal Oxidation Profiling of Single-Walled Carbon Nanotubes. *Chem. Mater.* **2005**, *17*, 6819−6834.
(19) Wu, Z.; Chen, Z.; Du, X.; Logan, J. M.; Sippel, J.; Nikolou, M.; Kamaras, K.; Reynolds, J. R.; Tanner, D. B.; Hebard, A. F.; Rinzler, A. G. Transparent, Conductive Carbon Nanotube Films. *Science* **2004**, *305*, 1273−1276.
(20) Cress, C. D.; McMorrow, J. J.; Robinson, J. T.; Friedman, A. L.; Landi, B. Radiation Effects in Single-Walled Carbon Nanotube Thin-Film-Transistors. *IEEE Trans. Nucl. Sci.* **2010**, *57*, 3040−3045.
(21) Ziegler, J. F. Srim-2003. *Nucl. Instrum. Methods Phys. Res., Sect. B* **2004**, *219−220*, 1027−1036.
(22) Berger, H. Models for Contacts to Planar Devices. *Solid-State Electron.* **1972**, *15*, 145−158.
(23) Dresselhaus, M. S.; Dresselhaus, G.; Saito, R.; Jorio, A. Raman Spectroscopy of Carbon Nanotubes. *Phys. Rep.* **2005**, *409*, 47−99.
(24) Reeves, G.; Harrison, H. Obtaining the Specific Contact Resistance from Transmission Line Model Measurements. IEEE. *IEEE Electron Device Lett.* **1982**, *3*, 111−113.
(25) Stavitski, N.; van Dal, M.; Wolters, R.; Kovalgin, A.; Schmitz, J. Specific Contact Resistance Measurements of Metal-Semiconductor Junctions. *IEEE Int. Conf. Microelectron. Test Struct. Proc.* **2006**, 13−17.

DOI: 10.1021/acsami.6b14041
ACS Appl. Mater. Interfaces 2017, 9, 7406−7411